

## Article

# Catalytic Pyrolysis of Waste-Printed Circuit Boards Using a Cu/Fe Bimetal Synergistic Effect to Enhance Debromination

Jiahui Wang <sup>1,\*</sup>, Zhen Xi <sup>2</sup>, Bo Niu <sup>3</sup>, Ruitong Gao <sup>2</sup> and Zhenming Xu <sup>4</sup><sup>1</sup> College of Life Sciences, Qingdao University, Qingdao 266071, China<sup>2</sup> College of Chemistry and Chemical Engineering, Institute for Sustainable Energy and Resources, Qingdao University, Qingdao 266071, China; xz18863092282@163.com (Z.X.); gaoruitong@qdu.edu.cn (R.G.)<sup>3</sup> Key Laboratory of Farmland Ecological Environment of Hebei Province, College of Resources and Environmental Science, Hebei Agricultural University, Baoding 071000, China; niubo@hebau.edu.cn<sup>4</sup> School of Environmental Science and Engineering, Shanghai Jiao Tong University, Shanghai 200240, China; zmxu@sjtu.edu.cn

\* Correspondence: jhwang@qdu.edu.cn

**Abstract:** Deep and efficient debromination is a critical step in achieving environmentally friendly recycling and ensuring the sustainability of waste-printed circuit boards (WPCBs) because of their high toxicity and carcinogenicity. To this end, this study used a copper–iron (Cu/Fe) bimetal as a debromination agent to remove bromides from WPCBs using in situ catalytic pyrolysis technology. The results show that the maximum debromination efficiency was 97.14% under the following conditions: a Cu mole ratio of 0.20 (Cu/Fe-0.20), a Cu/Fe-0.20 dosage of 0.4, a pyrolysis temperature of 600 °C, and a retention time of 10 min. The main bromine species in pyrolysis oil and gas were bromophenol, bromomethane, HBr, and Br<sub>2</sub>. The conversion of bromine species and the debromination of the Cu/Fe-0.20 bimetal were analyzed in real time using a thermogravimetry-coupled Fourier transform infrared and mass spectrometer (TG-FTIR-MS). Using the Cu/Fe bimetal synergistic effect, we determined that the debromination mechanism could be used for bromide conversion and fixing. The Cu in the Cu/Fe-0.20 transformed the organic Br (bromophenol and bromomethane) into inorganic Br (HBr and Br<sub>2</sub>) by providing empty orbitals for lone pairs of electrons. Then, the generated HBr and Br<sub>2</sub> reacted with Fe in the Cu/Fe-0.20 and were fixed in pyrolysis residue. This study provides theoretical support and a practical method for WPCB deep debromination and recycling.



**Citation:** Wang, J.; Xi, Z.; Niu, B.; Gao, R.; Xu, Z. Catalytic Pyrolysis of Waste-Printed Circuit Boards Using a Cu/Fe Bimetal Synergistic Effect to Enhance Debromination. *Sustainability* **2024**, *16*, 3009. <https://doi.org/10.3390/su16073009>

Academic Editor: Adam Smoliński

Received: 27 February 2024

Revised: 28 March 2024

Accepted: 2 April 2024

Published: 4 April 2024



**Copyright:** © 2024 by the authors. Licensee MDPI, Basel, Switzerland. This article is an open access article distributed under the terms and conditions of the Creative Commons Attribution (CC BY) license (<https://creativecommons.org/licenses/by/4.0/>).

**Keywords:** waste-printed circuit boards; debromination; in situ catalytic pyrolysis; sustainability; Cu/Fe bimetal; mechanism

## 1. Introduction

Waste electrical and electronic equipment (WEEE) is a significant contaminant because of the large amounts produced, their complex components, and their high pollution levels. The global production of WEEE is considered to be more than 50 million tons, and the yield continuously increases by 10% every year [1]. Waste-printed circuit boards (WPCBs) are the most important constituent of WEEE and have dramatically increased with the production of WEEE [2]. WPCBs can comprise various metals (such as gold, silver, copper, iron, aluminum, etc.), organic matter (epoxy resin, plastic, phenolic resin, etc.), and hazardous substances (heavy metals, binders, and brominated flame retardants (BRFs)), all of which are valuable for “urban mines” [3]. Therefore, some researchers are committed to recycling valuable metals and have made significant achievements in this regard [4,5]. However, the safe disposal and recovery of residual nonmetals in WPCBs (NM-WPCBs) has been neglected. NM-WPCBs are a typical form of hazardous waste that contains a large number of BRFs [6]. Improper disposal methods such as landfilling and incineration can release polybrominated diphenyl ethers (PBDEs), Tetrabromobisphenol A (TBBPA), polycyclic aromatic hydrocarbons (PAHs), and brominated aromatic hydrocarbons, which can

accumulate in human bodies and cause serious diseases [7]. Therefore, the debromination of NM-WPCBs is necessary.

A few debromination technologies (such as supercritical fluid treatment, subcritical fluid method, in situ pyrolysis, the mechanochemical method, and the microbial method) have been adopted to remove hazardous substances and recycle valuable materials from NM-WPCBs [8–10]. Of these, in situ pyrolysis is one of the most promising technologies for bromine removal and sustainable resource recovery because of its obvious advantages. Firstly, toxic components such as PBDEs, TBBPA, and PAHs are not produced by in situ pyrolysis because of its oxygen-deficient atmosphere, and other bromine-containing substances such as bromophenol and hydrogen bromide can be simultaneously removed via the reactions of debromination agents. Secondly, NM-WPCBs can be decomposed into small molecular organics during the process, which can then be recycled as an alternative chemical feedstock. Thirdly, compared with supercritical fluid treatment, the subcritical fluid method, the mechanochemical method, and the microbial method, in situ pyrolysis is more efficient and is usable at relatively low temperatures and pressures, which can reduce energy consumption and costs. Considering the importance of environmental protection and resource recycling, researchers have devoted themselves to investigating the effectiveness of debromination using the in situ pyrolysis method [11–13]. Zhu et al. accurately calculated the capture capacity and mechanisms of  $\text{CaCO}_3$  for bromides generated when using the pyrolysis process on brominated resin but found that the capture capacity of  $\text{CaCO}_3$  for  $\text{CH}_3\text{Br}$  was only  $2.37 \times 10^{-9}$  mol/g. Gao et al. removed bromides from WPCBs via the in situ pyrolysis of  $\text{Ca}(\text{OH})_2$ , and the results showed that all HBr species and nearly 75% of organic bromide species (such as bromophenol, 4-bromophenol, and 2,4-dibromophenol) were successfully removed. Bhaskar et al. used a calcium hydroxide carbon composite as a debromination agent to remove bromide from Br-containing plastic, and they found that most of the bromides were absorbed and removed [14,15]. Ma et al. enhanced debromination performance by adding Fe particles to ZSM-5 and Ni/SiO<sub>2</sub>-Al<sub>2</sub>O<sub>3</sub> catalysts, and the results showed that the bromine content in the oils was reduced by between 8.74 wt% and 5.96 wt% and between 8.74 wt% and 5.46 wt%, respectively [16,17]. However, removing organic bromide species generated by pyrolysis is difficult. Taking into consideration the damage caused by organic bromides, the deep and complete debromination of WPCBs is necessary.

Metal catalysts are one of the agents used for WPCB debromination [7,18]. Mono-metals such as iron, zinc, nickel, and their oxides are used to remove Br from WPCBs. Studies suggest that most inorganic bromides, such as HBr and Br<sub>2</sub>, can be efficiently removed. However, the removal efficiency for organic bromides such as bromomethane and bromophenol is low. However, bimetal catalysts have several apparent advantages and thus have the potential to remove Br from WPCBs. Bimetal agents can promote pyrolysis reactions by facilitating heat transfer. Furthermore, bimetal debromination agents can simultaneously remove organic and inorganic bromides via chemical and physical reactions. Therefore, some studies on debromination via bimetals have been carried out. Ma et al. found that zero-valent Fe and Ni can capture evolved bromides from WPCBs via two-stage catalytic pyrolysis. Terakado et al. investigated the debromination ability of metal oxides such as Fe<sub>2</sub>O<sub>3</sub> and ZnO and found that these catalysts have obvious debromination efficiency with HBr and organic bromine compounds. However, previous studies have mainly focused on debromination efficiency. The synergistic debromination mechanism of bimetal catalysts is unclear [19,20], and the removal of organic bromides needs to be improved. Our previous study found that copper has excellent removal efficiency with organic bromides and Fe has advantages in removing Br<sub>2</sub> and HBr. Therefore, Cu/Fe has great potential regarding WPCB deep debromination.

Thus, this study used the in situ catalytic pyrolysis techniques with Cu/Fe bimetal and WPCBs to investigate the performance and mechanisms of debromination. Firstly, the Cu/Fe bimetal was prepared and characterized using a high-resolution transmission electron microscope (HRTEM), X-ray diffraction (XRD), and X-ray photoelectron spectroscopy

(XPS). Then, debromination efficiency and performance factors were investigated to obtain optimal parameters. The debromination process and products were analyzed in real time with TG-FTIR-MS. Based on these results, a deep debromination mechanism was proposed. This study provides a new method and theoretical support for WPCB deep debromination and recycling.

## 2. Experimental Section

### 2.1. Materials

WPCBs were collected from Qingdao Rong Yiyang Resource Recycle Company and pre-treated, as shown in Figure 1. Firstly, the WPCBs were disassembled to recycle their electron components. Then, the residual mainboards were frozen with liquid nitrogen and crushed into a fine powder. Afterwards, the powder was separated via magnetic separation to recover metal resources. The resulting residual NM-WPCBs with a size distribution ranging from 0.15 to 0.60 mm, were the experimental samples used in this study (Figure S1). The main element components of the NM-WPCBs were C, H, O, Br, Si, and Ca. Sodium borohydride ( $\text{NaBH}_4$ ) and ferric chloride hexahydrate ( $\text{FeCl}_3 \cdot 6\text{H}_2\text{O}$ ) were purchased from Sinopharm Group Co., Ltd. Copper sulfate pentahydrate ( $\text{CuSO}_4 \cdot 5\text{H}_2\text{O}$ ) was obtained from Aladdin Reagents Co., Ltd. All chemicals used in this study were analytic grade and had no further treatments.

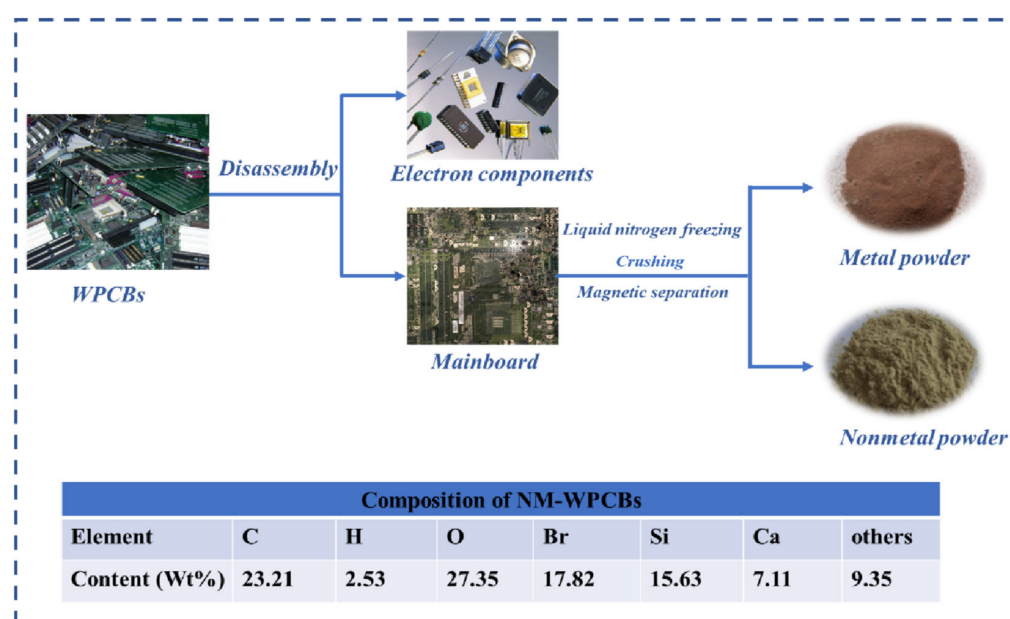


**Figure 1.** Pretreatment process and main composition of NM-WPCBs.

### 2.2. Preparation of Cu/Fe

Cu/Fe was synthesized via precipitation and displacement. Briefly,  $\text{N}_2$  was pumped into 0.05 mol/L  $\text{FeCl}_3 \cdot 6\text{H}_2\text{O}$  to fully remove  $\text{O}_2$  from the solution. Then, 0.10 mol/L  $\text{NaBH}_4$  was added drop by drop at 500 rpm until the mixture turned black.  $\text{Fe}^{3+}$  was reduced to Fe as per Equation (1):



Then, 0.05 mol/L  $\text{CuSO}_4 \cdot 5\text{H}_2\text{O}$  was added to the mixture with different Fe and Cu mole ratios (0, 1.05:0.05, 1.10:0.10, 1.20:0.20, and 1.50:0.50) at 250 rpm for 30 min. Cu was deposited on the surface of Fe to obtain Cu/Fe, as shown in Equation (2):



The Cu/Fe was washed three times using ethanol (Cu) and deionized water (Fe) under a N<sub>2</sub> atmosphere. Finally, the Cu/Fe was dried with a freeze dryer for 48 h, and passivation was achieved using 1.0% O<sub>2</sub>. According to a mass balance calculation, the mole ratios of Cu in the prepared Cu/Fe were 0 (Cu/Fe-0), 0.05 (Cu/Fe-0.05), 0.10 (Cu/Fe-0.10), 0.20 (Cu/Fe-0.20), and 0.50 (Cu/Fe-0.50).

### 2.3. In Situ Catalytic Pyrolysis Experiment

The in situ catalytic pyrolysis experiments were carried out in a self-designed tube furnace (Figure S2). In a typical run, 5.00 g NM-WPCBs were fully mixed with a certain amount of Cu/Fe and put in a quartz boat. Then, the quartz boat was placed in the heating zone of the tube furnace. Before the start of the experiment, Ar was pumped into the quartz tube for 20 min to completely exhaust the air. After that, the samples were heated to the designed temperature (400, 450, 500, 550, 600, 650, and 700 °C) at 10 °C/min and held at that temperature for 30 min to ensure that the in situ catalytic pyrolysis reaction was thoroughly completed. Finally, the produced pyrolysis oil was condensed and collected in a liquid collector, while pyrolysis gas was obtained by gas collector.

The total debromination efficiency was calculated using Equation (3):

$$\eta_{(d-Br)} = W_{(s)} / W_{(0)} \times 100\% \quad (3)$$

where  $\eta_{(d-Br)}$  is the debromination efficiency (%);  $W_{(s)}$  is the bromine mass in the pyrolysis residue (mg);  $W_{(0)}$  is the bromine mass in the NM-WPCBs (mg).

The removal efficiency for organic Br and inorganic Br were determined by Equations (4) and (5):

$$\eta_{(or-Br)} = (1 - W_{(or-Br)} / W_{(T-or)}) \times 100\% \quad (4)$$

$$\eta_{(in-Br)} = (1 - W_{(in-Br)} / W_{(T-in)}) \times 100\% \quad (5)$$

where  $\eta_{(or-Br)}$  and  $\eta_{(in-Br)}$  are the removal efficiency of organic Br and inorganic Br (%);  $W_{(or-Br)}$  is the mass of organic Br in the pyrolysis oil (mg);  $W_{(in-Br)}$  is the mass of inorganic Br in the pyrolysis oil and gas (mg).  $W_{(T-or)}$  is the mass of organic Br in the pyrolysis oil without adding Cu/Fe (mg); and  $W_{(T-in)}$  is the mass of inorganic Br in the pyrolysis oil and gas without adding Cu/Fe (mg).

### 2.4. Characterization

The microstructure and morphology of Cu/Fe were characterized by high-resolution transmission electron microscope (HRTEM, TecnaiF20, The Netherlands). The crystalline structures and composition of Cu/Fe were determined by X-ray diffraction (XRD, Bruker D8 Advance, Germany) and X-ray photoelectron spectroscopy (XPS, Thermo Fisher K-Alpha 250XI, USA). The bromine content in the NM-WPCBs and pyrolysis products were measured by oxygen bomb combustion coupled with iron chromatography (IC, Essentia IC-16, Japan). And organic bromides in pyrolysis oil and gas were analyzed by gas chromatograph-mass spectroscopy (GC-MS, QP2010, Shimadzu, Japan). The debromination process was determined by thermogravimetric Fourier transform infrared spectrometer-mass spectroscopy (TG-FTIR-MS, TGA8000-Frontier-Clarus 680-Clarus SQ 8T, USA).

## 3. Results and Discussion

### 3.1. Characterization of Cu/Fe

HRTEM was used to analyze the morphology and size of Cu/Fe-0.20. Figure 1a shows that the Cu/Fe mainly comprised small core-shell spheres with an average size ranging from 30 to 50 nm. These spheres assembled with each other to form a large aggregation with a chain structure. Furthermore, a high-magnification image of the Cu/Fe showed that the Cu was loaded on the surface of the Fe particles (Figure 2b). To further clarify the microstructure of the Cu/Fe, an energy-dispersive X-ray spectrometer (EDS) image was created (Figure 2c–e). It showed that the Cu and Fe could be observed simultaneously and had the same distribution, which further suggested that the Cu was successfully loaded on

the surface of the Fe, forming core–shell structures. Furthermore, a small amount of O was observed, which indicated that the Cu/Fe was slightly oxidized.

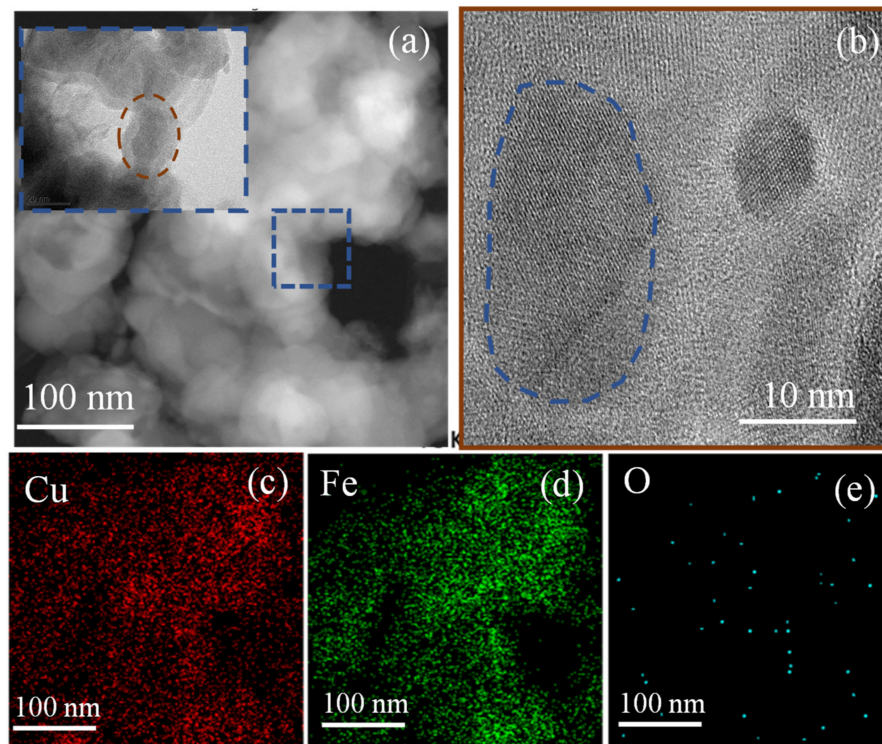


**Figure 2.** HRTEM and element mapping of the prepared Cu/Fe-0.20. (a,b) the TEM of Cu/Fe-0.20; (c–e) the element mapping of Cu, Fe, O of Cu/Fe-0.20.

To investigate the crystalline structure, surface composition, and chemical state of the Cu/Fe, XRD and XPS analyses were carried out. Figure 3a shows the XRD patterns of the sample, indicating the presence of  $\text{Cu}^0$  (JCPDS card no: 04-0836),  $\text{Fe}^0$  (JCPDS card no: 34-0529),  $\text{Cu}_2\text{O}$  (JCPDS card no: 05-0667),  $\text{FeO}$  (JCPDS card no: 06-0615), and  $\text{Fe}_3\text{O}_4$  (JCPDS card no: 26-1136). The XRD pattern of the  $\text{Cu}_2\text{O}$  suggested that the  $\text{Cu}^0$  on the surface was slightly oxidized, while the presence of  $\text{FeO}$  and  $\text{Fe}_3\text{O}_4$  indicated that the  $\text{Fe}^0$  was also oxidized. The simultaneous presence of Cu and Fe indicated the successful preparation of Cu/Fe. Furthermore, the XPS technique was used to analyze the surface composition and chemical state of the sample. Figure 3b shows a survey scan spectrum of the main signals of Cu, Fe, O, and C. High-resolution spectra of Cu 2p and Fe 2p are presented in Figures 3c and 3d, respectively. The binding energies located at 934.5 eV and 953.1 eV were assigned to Cu 2p<sub>3/2</sub> and Cu 2p<sub>1/2</sub>, which indicated the presence of  $\text{Cu}^0$  [21], and a strong  $\text{Cu}^{2+}$  satellite was observed with a binding energy of 942.4 eV. Furthermore, the binding energies at 935.1 eV and 954.6 eV could be attributed to Cu 2p<sub>3/2</sub> and Cu 2p<sub>1/2</sub> in the CuO, which suggested that the Cu was oxidized. Figure 3d shows that the binding energies located at 710.2 eV and 724.4 eV were assigned to  $\text{Fe}^{2+}$ , and the binding energies at 711.3 eV and 726.7 eV were assigned to  $\text{Fe}^{3+}$  [22]. These results indicate that the  $\text{Fe}^0$  on the surface of Cu/Fe was oxidized into  $\text{FeO}$  and  $\text{Fe}_3\text{O}_4$ , which was consistent with the results of XRD.

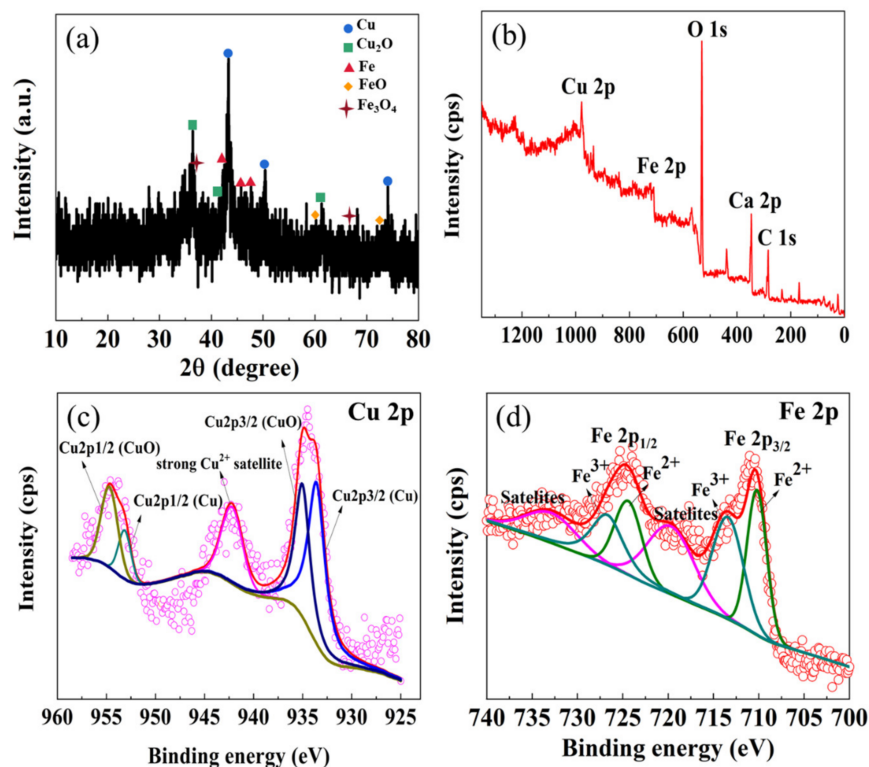


**Figure 3.** (a) XRD and (b–d) XPS analyses of Cu/Fe-0.20.

### 3.2. Factors on In Situ Catalytic Pyrolysis Debromination

Figure 4 shows the Cu mole ratio's influence on the bimetal, Cu/Fe dosage, reaction temperature, and retention time with respect to organic and inorganic bromide debromination and removal efficiency. Figure 4a shows that the debromination efficiency significantly increased from 52.32% to 95.10% when the mole ratio of Cu increased to 0.20. At the same time, the removal efficiency for inorganic Br was up to 94.22% and remained almost unchanged, while the removal efficiency for organic Br increased from 60.12% to 90.11%. This phenomenon indicated that the presence of Cu enhances Cu/Fe debromination via the catalytic effect. During in situ catalytic pyrolysis, any organic Br generated (such as 1-bromophenol, 4-bromophenol, or 1,4-bibromophenol) can be transformed into HBr and Br<sub>2</sub> via the catalytic effect of Cu, while inorganic Br from NM-WPCBs can be removed with Fe through a reaction between HBr and Fe [17,23]. When the mole ratio of Cu is higher than 0.2, the debromination efficiency slightly decreases with an increase in Cu. At this point, the removal efficiency for organic Br was 90.21% and was almost unchanged by the increase in Cu. However, the removal efficiency for inorganic Br decreased from 94.22% to 63.56%. This result indicates that too much Cu in Cu/Fe is bad for the debromination reaction because of Fe coverage, which inhibits the reaction between inorganic Br and Fe. Moreover, the effect of the Cu mole ratio on the yield of pyrolysis oil, gas, and residue was also analyzed, as shown in Figure 4b. The increase in the Cu mole ratio did not affect the yields of pyrolysis oil, gas, or residue, and these results suggest that the Cu in Cu/Fe has little effect on the adsorption of pyrolysis oil and gas. Thus, the pyrolysis oil, gas, and residue yields were nearly unchanged. Therefore, the best catalyst was Cu/Fe-0.20.

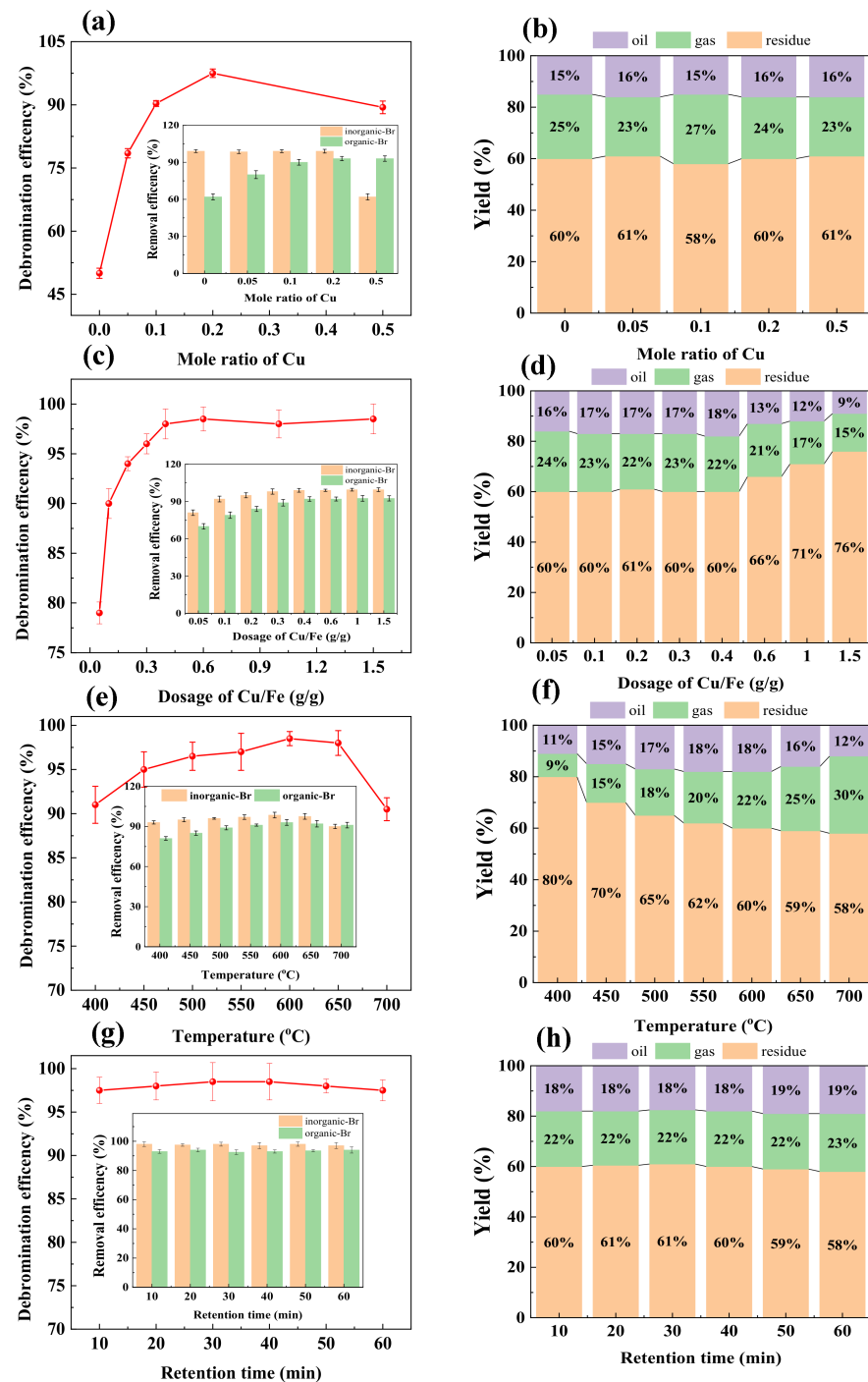


**Figure 4.** Effect of (a,b) mole ratio of Cu (dosage of Cu/Fe, 0.6; reaction temperature, 600 °C; retention time, 30 min), (c,d) dosage of Cu/Fe (Cu/Fe-0.20; reaction temperature, 600 °C; retention time, 30 min), (e,f) reaction temperature (Cu/Fe-0.20; dosage of Cu/Fe, 0.4; retention time, 30 min), and (g,h) retention time (Cu/Fe-0.20; dosage of Cu/Fe, 0.4; reaction temperature, 600 °C) on the debromination efficiency and yield of pyrolysis oil, gas, and residue.

The Cu/Fe-0.20 dosage was an important factor influencing the debromination process in our study. Figure 4c shows that the debromination efficiency significantly increased from 77.25% to 95.42% when the Cu/Fe-0.20 dosage increased from 0.05 to 0.40. At this time, the removal efficiencies for inorganic Br and organic Br increased with the increase in Cu/Fe-0.20 dosage. This result suggests that increased Cu/Fe-0.20 dosage was conducive to debromination because of the abundant active bromide removal sites. The continuous

increase in Cu/Fe-0.20 had little influence on debromination efficiency; the total debromination efficiency was 95.34% and hardly changed as the Cu/Fe-0.20 dosage increased. However, the pyrolysis oil and gas yields distinctly decreased with a Cu/Fe-0.20 dosage higher than 0.40 (Figure 4d), indicating that too much Cu/Fe-0.20 hinders the generation and release of pyrolysis oil and gas. During in situ catalytic pyrolysis, the reaction between Fe and inorganic Br can form defects in Cu/Fe-0.20 catalysts, which may adsorb the pyrolysis oil and gas and transform them into char [17]. Thus, the pyrolysis oil and gas yields decreased, and therefore, the optimal Cu/Fe-0.20 dosage for debromination was 0.4.

Figure 4e shows the effect of pyrolysis temperature on debromination efficiency. When the temperature increased from 400 °C to 600 °C, the debromination efficiency slightly increased from 91.52% to 97.23%. At this time, the removal efficiency of organic Br increased from 82.31% to 90.15%, and the removal efficiency for inorganic Br was almost unchanged at 95.02%. This result suggests that a high temperature can increase the catalytic activity of Cu/Fe-0.20, which could cleave the C-Br bond and increase the removal efficiency for inorganic Br. However, when the pyrolysis temperature was higher than 600 °C, the debromination efficiency decreased. At this stage, the formed FeBr<sub>2</sub>/FeBr<sub>3</sub> decomposed, generated inorganic Br, and was released into the pyrolysis oil and gas (Figure S3). Thus, the removal efficiency for inorganic Br and the total debromination efficiency decreased [24]. Moreover, a high temperature could promote secondary thermal cracking in pyrolysis oil. Thus, when the temperature was higher than 600 °C, the pyrolysis oil yield decreased from 18% to 12%, while the pyrolysis gas yield significantly increased to 30% (Figure 4f). Therefore, 600 °C was the optimal in situ catalytic pyrolysis temperature for WPCB debromination.

Retention time is an influential parameter in the debromination process. Figure 4g shows retention time's influence on debromination efficiency. When the retention time increased from 10 to 60 min, debromination efficiency for the WPCBs was 97.14% and almost unchanged. At the same time, the removal efficiency for organic Br and inorganic Br was high. These results indicate that the speed of catalysis for Cu/Fe-0.20 was fast, and the debromination reaction could be completed within 10 min. Moreover, the pyrolysis residue yield slightly decreased, while the pyrolysis gas yield increased because of the secondary pyrolysis, which may result in more complicated pyrolysis gas components (Figure 4h). Therefore, with respect to energy consumption, a retention time of 10 min is suitable for in situ pyrolysis debromination.

With a comprehensive analysis of debromination efficiency, energy consumption, and cost, we found that a Cu mole ratio of 0.20, a Cu/Fe-0.20 dosage of 0.4, a pyrolysis temperature of 600 °C, and a retention time of 10 min are the optimal parameters for catalytic pyrolysis debromination. Under optimal conditions, the debromination efficiency was up to 97.14%.

### 3.3. In Situ Pyrolysis Catalytic Products

Tables S1 and S2 show the compositions of pyrolysis oil and gas after the in situ catalytic pyrolysis of NM-WPCBs and Cu/Fe-0.20. The debromination products were complex. The pyrolysis oil mainly comprised phenol, methyl phenol, ethyl phenol, isopropenylphenol, and benzene, while pyrolysis gas mainly comprised aldehyde, carbon dioxide, propanal, and water. However, small organic Br compounds, such as bromophenol and bromomethane, were detected in the pyrolysis oil and gas, and organic Br content was reduced compared with that of NM-WPCBs [25]. Therefore, most bromides can be removed by Cu/Fe-0.20 via in situ catalytic pyrolysis.

To clarify the Cu/Fe-0.20 debromination process in detail, a real-time analysis of bromine species generated from NM-WPCBs was carried out via TG-FTIR and TG-MS technologies. Figure 5 and Table S4 show the TG-FTIR spectrum of volatile products produced during the in situ catalytic pyrolysis of NM-WPCBs and Cu/Fe-0.20. Characteristic bands at 3600–3900, 2850–3100, 2300–2400, 1600–1800, 1300–1500, and 550–750 cm<sup>-1</sup> were observed when the in situ catalytic pyrolysis temperature was higher than 300 °C, which indicated

that pyrolysis and debromination reactions occurred at this case. The strong adsorption bands at 3600–3900  $\text{cm}^{-1}$  were attributed to the stretching vibrations of O-H in phenols and  $\text{H}_2\text{O}$  [26]. The adsorption bands at 2300–2400  $\text{cm}^{-1}$  were the stretching vibrations of  $\text{O}=\text{C}=\text{O}$  in carbon dioxide [24]. The characteristic bands ranging from 2800 to 3000  $\text{cm}^{-1}$  were assigned to the stretching vibrations of C-H in alkane and its substituents [27]. The adsorption bands at 1600–1800  $\text{cm}^{-1}$  were the stretching vibrations of aromatic C=C in benzene and phenol rings. The characteristic bands at 1300–1500  $\text{cm}^{-1}$  were attributed to the in-plane bending of O-H in phenol [28]. Finally, the bands at 550–750  $\text{cm}^{-1}$  were attributed to the bending vibrations of C-Br in brominated phenols. However, the characteristic HBr bands at 2500–2600  $\text{cm}^{-1}$  were not observed, which suggested that the generated HBr was successfully removed by Cu/Fe-0.20. It should be noted that the strength of the characteristic bands significantly decreased when the temperature was higher than 450  $^{\circ}\text{C}$ , which indicated that the debromination reaction was nearly finished.

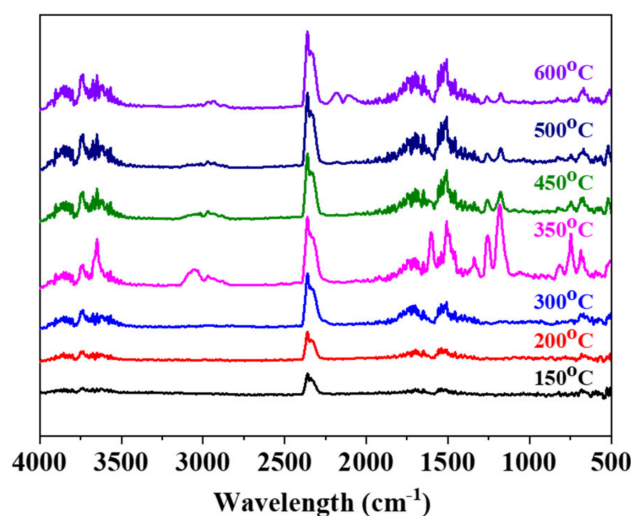


**Figure 5.** TG-FTIR spectrums of in-situ catalytic pyrolysis products for NM-WPCBs and Cu/Fe-0.20.

To better understand the debromination process of Cu/Fe-0.20, TG-MS was employed to investigate the generation and removal of inorganic Br and organic Br in real time. Figure 6a,b shows strong characteristic HBr and  $\text{Br}_2$  peaks during Cu catalysis when the temperature is higher than 300  $^{\circ}\text{C}$ . These peaks appear as a bimodal distribution, which may be attributable to an Ullmann cross-coupling reaction caused by Cu [29], which could generate inorganic Br. However, these signal intensities noticeably weakened after Cu/Fe-0.20 catalysis, which indicated that the HBr and  $\text{Br}_2$  were successfully removed via Cu/Fe-0.20 through catalysis and chemical reaction. Figure 6c,d shows the mass spectrums of bromomethane and bromophenol. The signal intensities of the bromomethane and bromophenol weakened after Cu/Fe-0.20 catalysis. This result suggests that Cu/Fe-0.20 can also remove organic Br. Indeed, Cu can cleave the C-Br bond and transform organic Br into inorganic Br. Furthermore, Fe can further remove any generated HBr or  $\text{Br}_2$  via chemical processes. Therefore, Cu/Fe-0.20 has excellent performance regarding organic Br and inorganic Br removal.

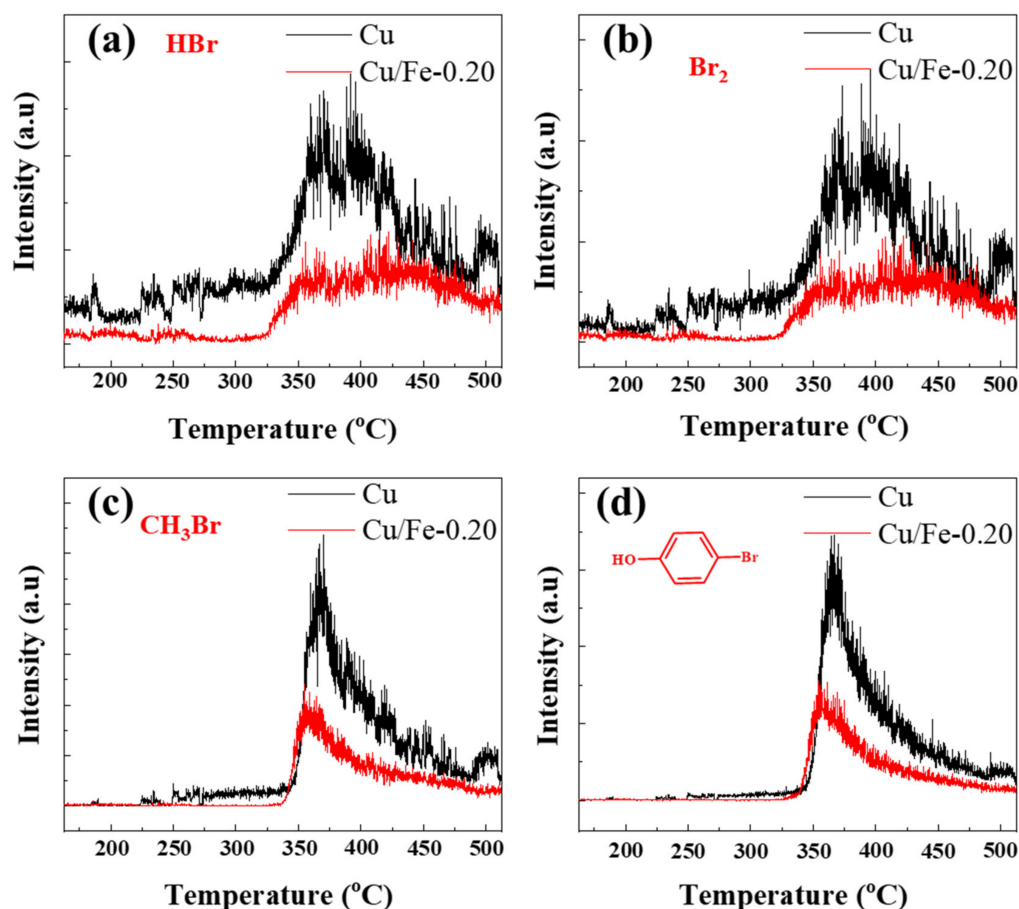


**Figure 6.** TG-MS spectrums of in situ catalytic pyrolysis products for NM-WPCBs and Cu/Fe-0.20 under Ar atmosphere: (a) HBr ( $m/z = 80$ ), (b) bromine gas ( $m/z = 158$ ), (c) bromoethane ( $m/z = 94$ ), and (d) 4-bromophenol (172).

### 3.4. Debromination Mechanism

Based on the GCMS and TG-FTIR-MS results, the debromination mechanism of Cu/Fe-0.20 is proposed in Figure 7. The Cu/Fe-0.20 debromination process can be divided into bromide conversion and fixing stages. When the temperature was higher than 300 °C, the NM-WPCBs decomposed into small molecular compounds such as phenol and its homologs, bromophenol, HBr, and Br<sub>2</sub>. At the bromide conversion stage, the Cu in the Cu/Fe bimetal converted organic Br into inorganic Br through catalysis (Equations (6)–(9)). The organic Br adsorbed the Cu atom to form [Organic-Br···Cu] by providing empty orbitals for lone pairs of electrons (Equation (6)). Then, the electrons transformed into [Organic-Br···Cu], cleaving the C-Br bond and forming a Cu···Br\* intermediate (Equation (7)). The generated Br\* reacted with Br\* and H\* to produce Br<sub>2</sub> and HBr (Equations (8) and (9)). Therefore, the Cu in the Cu/Fe transformed the organic Br into inorganic Br. It should be noted that the formation of metal–oxide interfaces as reactive sites, such as Cu-FeOx interfaces, may promote organic Br removal [30–32].

At the fixing stage, the generated Br<sub>2</sub> and HBr reacted with Fe, Fe<sub>3</sub>O<sub>4</sub>, and Cu<sub>2</sub>O (Equations (10)–(13)). According to our calculations, the Fe<sub>3</sub>O<sub>4</sub> and Cu<sub>2</sub>O fixed the inorganic Br (Figure S3). Indeed, the reaction between the inorganic Br and Fe, Fe<sub>3</sub>O<sub>4</sub>, and Cu<sub>2</sub>O included dissociative adsorption, the formation of intermediates such as oxyhalide structures (copper halide and iron halide), and the desorption process [33,34]. Through these reactions, the organic Br and inorganic Br in the pyrolysis products were removed. The encapsulation of metallic sites caused by the oxide layer may result in a strong metal–support interaction. Therefore, the stability of this catalyst could be improved. And the

encapsulation of metallic sites by the oxide layer may result in a strong metal support interaction [35,36]. Therefore, the stability of this catalyst could be improved.

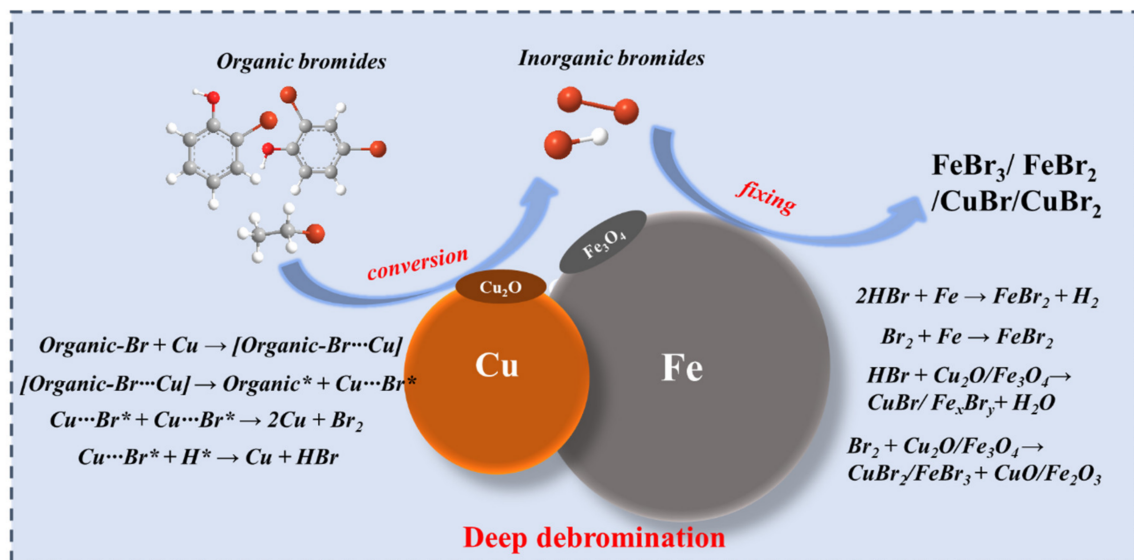
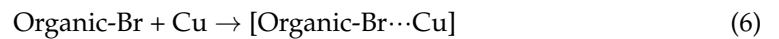


Figure 7. Deep debromination mechanism for in situ catalytic pyrolysis of Cu/Fe-0.20 and WPCBs.

#### 4. Conclusions

We prepared a Cu/Fe bimetal and used it to remove brominated flame retardants from WPCBs via in situ catalytic pyrolysis. Our HRTEM, XRD, and XPS results suggest that a Cu/Fe bimetal with a core-shell structure was successfully synthesized. The maximum debromination efficiency reached 97.14% when the Cu mole ratio was 0.20, the Cu/Fe-0.20 dosage was 0.4, the pyrolysis temperature was 600 °C, and the retention time was 10 min. Under these conditions, the pyrolysis oil and gas yields were 18% and 22%, respectively. The debromination products and mechanism of Cu/Fe-0.20 were analyzed in real time via TG-FTIR-MS. During in situ catalytic pyrolysis, the Cu in Cu/Fe-0.20 transformed organic Br into inorganic Br, while the Fe further fixed inorganic Br in the residue. The Br atom in organic Br species (bromophenol and bromomethane) coordinated with the Cu by providing lone pair electrons to form [Organic-Br⋯Cu], which weakened the strength of the C-Br bond and made it easy to cleave. Thus, the organic Br was transformed into inorganic Br species such as HBr and Br<sub>2</sub> with Cu catalysis. Then, the generated inorganic Br was fixed in pyrolysis residue with an Fe reaction. Therefore, the organic Br and inorganic Br in the pyrolysis products were removed.

**Supplementary Materials:** The following supporting information can be downloaded at: <https://www.mdpi.com/article/10.3390/su16073009/s1>, Figure S1: Size distribution of NM-WPCBs. Figure S2: Schematic illustration of co-pyrolysis apparatus. Figure S3: The relationship between  $\Delta G$  and temperature for the reaction of catalysts. Figure S4: The spectrum of TG-FIIR at 150, 350 and 450 °C. Figure S5: The relationship between  $\Delta G$  and temperature for the debromination of catalysts. Table S1: Main compositions of pyrolysis liquid for co-pyrolysis of NM-WPCBs and Cu/Fe-0.20. Table S2: Main compositions of pyrolysis gas for co-pyrolysis of NM-WPCBs and Cu/Fe-0.20.

**Author Contributions:** J.W.: writing—original draft, conceptualization, methodology, investigation. Z.X. (Zhen Xi): investigation, supervision, resources. B.N.: conceptualization, methodology, funding acquisition. R.G.: writing—reviewing and editing, conceptualization, methodology, funding acquisition. Z.X. (Zhenming Xu): visualization, supervision. All authors have read and agreed to the published version of the manuscript.

**Funding:** This work was supported by the Natural Science Foundation of Shandong Province [ZR2022QE042] and China Petroleum Science and Technology Innovation Fund [2021DQ02-0603].

**Data Availability Statement:** Data are contained within the article.

**Conflicts of Interest:** The authors declare that they have no conflicts of interest.

## References

1. Awasthi, A.; Zlamparet, G.; Zeng, X.; Li, J. Evaluating waste printed circuit boards recycling: Opportunities and challenges, a mini review. *Waste Manag. Res.* **2017**, *35*, 346–356. [[CrossRef](#)] [[PubMed](#)]
2. Ning, C.; Lin, C.; Hui, D.; McKay, G. Waste Printed Circuit Board (PCB) Recycling Techniques. *Topics Curr. Chem.* **2017**, *375*, 43. [[CrossRef](#)] [[PubMed](#)]
3. Zhu, J.; Chen, X.; Yao, Z.; Yin, Y.; Lin, K.; Liu, H.; Huang, J.; Ruan, J.; Qiu, R. Directional concentration of bromine from nonmetallic particles of crushed waste printed circuit boards by vacuum-gasification-condensation. *J. Clean. Prod.* **2019**, *231*, 462–467. [[CrossRef](#)]
4. Li, H.; Eksteen, J.; Oraby, E. Hydrometallurgical recovery of metals from waste printed circuit boards (WPCBs): Current status and perspectives—A review. *Resour. Conserv. Recy.* **2018**, *139*, 122–139. [[CrossRef](#)]
5. Zhu, P.; Chen, Y.; Hao, Y.; Fan, Z.Y.; Qian, G.R.; Zhou, M. Leaching behavior of copper powders from waste printed circuit board by electrogenerated chlorine and aeration. *Mining Metall. Explora.* **2013**, *30*, 79–84. [[CrossRef](#)]
6. Hu, D.; Jia, Z.; Li, J.; Zhong, B.; Fu, W.; Luo, Y.; Jia, D. Characterization of Waste Printed Circuit Boards Nonmetals and its Reutilization as Reinforcing Filler in Unsaturated Polyester Resin. *J. Polym. Environ.* **2018**, *26*, 1311–1319. [[CrossRef](#)]
7. Huang, Z.; Deng, D.; Qiao, J.; Ju, Y.; Chen, Y.; Dionysiou, D.D. New insight into the cosolvent effect on the degradation of tetrabromobisphenol A (TBBPA) over millimeter-scale palladised sponge iron (Pd-s-Fe<sup>0</sup>) particles. *Chem. Eng. J.* **2019**, *361*, 1423–1436. [[CrossRef](#)]
8. Ma, C.; Yu, J.; Wang, B.; Song, Z.; Xiang, J.; Hu, S.; Su, S.; Sun, L. Chemical recycling of brominated flame retarded plastics from e-waste for clean fuels production: A review. *Renew. Sust. Energ. Rev.* **2016**, *61*, 433–450. [[CrossRef](#)]
9. Altarawneh, M.; Saeed, A.; Al-Harashsheh, M.; Dlugogorski, B.Z. Thermal decomposition of brominated flame retardants (BFRs): Products and mechanisms. *Prog. Energ. Combust.* **2019**, *70*, 212–259. [[CrossRef](#)]
10. Liu, W.; Xu, J.; Han, J.; Jiao, F.; Qin, W.; Li, Z. Kinetic and Mechanism Studies on Pyrolysis of Printed Circuit Boards in the Absence and Presence of Copper. *ACS Sustain. Chem. Eng.* **2018**, *7*, 1879–1889. [[CrossRef](#)]
11. Qin, B.; Lin, M.; Chen, X.; Xu, Z.; Fu, Y.; Hu, J.; Ruan, J. A novel approach for determining the accurate debromination time in the ball-milling process of nonmetallic particles from waste printed circuit boards by computation. *J. Hazard. Mater.* **2021**, *410*, 124611. [[CrossRef](#)] [[PubMed](#)]
12. Qin, B.; Lin, M.; Yao, Z.; Zhu, J.; Ruan, J.; Tang, Y.; Qiu, R. A novel approach of accurately rationing adsorbent for capturing pollutants via chemistry calculation: Rationing the mass of CaCO<sub>3</sub> to capture Br-containing substances in the pyrolysis of nonmetallic particles of waste printed circuit boards. *J. Hazard. Mater.* **2020**, *393*, 122410. [[CrossRef](#)] [[PubMed](#)]
13. Ma, C.; Yu, J.; Chen, T.; Yan, Q.; Song, Z.; Wang, B.; Sun, L. Influence of Fe based ZSM-5 catalysts on the vapor intermediates from the pyrolysis of brominated acrylonitrile-butadiene-styrene copolymer (Br-ABS). *Fuel* **2018**, *230*, 390–396. [[CrossRef](#)]
14. Bhaskar, T.; Matsui, T.; Kaneko, J.; Uddin, M.A.; Muto, A.; Sakata, Y. Novel calcium based sorbent (Ca-C) for the dehalogenation (Br, Cl) process during halogenated mixed plastic (PP/PE/PS/PVC and HIIPS-Br) pyrolysis. *Green Chem.* **2002**, *4*, 372–375. [[CrossRef](#)]
15. Bhaskar, T.; Negoro, R.; Muto, A.; Sakata, Y. Prevention of chlorinated hydrocarbons formation during pyrolysis of PVC or PVDC mixed plastics. *Green Chem.* **2006**, *8*, 697. [[CrossRef](#)]
16. Ma, C.; Kamo, T. Enhanced debromination by Fe particles during the catalytic pyrolysis of non-metallic fractions of printed circuit boards over ZSM-5 and Ni/SiO<sub>2</sub>-Al<sub>2</sub>O<sub>3</sub> catalyst. *J. Anal. Appl. Pyrol.* **2019**, *138*, 170–177. [[CrossRef](#)]
17. Ma, C.; Kamo, T. Effect of steam-iron reaction on product characteristics and debromination during pyrolysis of epoxy-printed circuit boards. *J. Hazard. Mater.* **2019**, *379*, 120803. [[CrossRef](#)] [[PubMed](#)]

18. Li, Y.; Li, X.; Xiao, Y.; Wei, C.; Han, D.; Huang, W. Catalytic debromination of tetrabromobisphenol A by Ni/nZVI bimetallic particles. *Chem. Eng. J.* **2016**, *284*, 1242–1250. [[CrossRef](#)]
19. Li, Q.; Wang, F.; Wang, F.; Bai, B.; Zhang, J.; Li, C.; Sun, Q.; Wang, Y.; Forson, K. Adsorption behavior and mechanism analysis of siloxane thickener for CO<sub>2</sub> fracturing fluid on shallow shale soil. *J. Mol. Liq.* **2023**, *376*, 121394. [[CrossRef](#)]
20. Li, O.; Liu, J.; Wang, S.; Guo, Y.; Han, X.; Li, Q.; Cheng, Y.; Dong, Z.; Li, X.; Zhang, X. Numerical insights into factors affecting collapse behavior of horizontal wellbore in clayey silt hydrate-bearing sediments and the accompanying control strategy. *Ocean Eng.* **2024**, *297*, 117029. [[CrossRef](#)]
21. Zhu, F.; Li, L.; Ma, S.; Shang, Z. Effect factors, kinetics and thermodynamics of remediation in the chromium contaminated soils by nanoscale zero valent Fe/Cu bimetallic particles. *Chem. Eng. J.* **2016**, *302*, 663–669. [[CrossRef](#)]
22. Li, Y.; Li, X.; Han, D.; Huang, W.; Yang, C. New insights into the role of Ni loading on the surface structure and the reactivity of nZVI toward tetrabromo- and tetrachlorobisphenol A. *Chem. Eng. J.* **2017**, *311*, 173–182. [[CrossRef](#)]
23. Lei, M.; Guo, S.; Wang, Z.; Zhu, L.; Tang, H. Ultrarapid and Deep Debromination of Tetrabromodiphenyl Ether over Noble-Metal-Free Cu/TiO<sub>2</sub> Nanocomposites under Mild Conditions. *Environ. Sci. Technol.* **2018**, *52*, 11743–11751. [[CrossRef](#)] [[PubMed](#)]
24. Liu, J.; Wang, H.; Zhang, W.; Wang, T.; Mei, M.; Chen, S.; Li, J. Mechanistic insights into catalysis of in-situ iron on pyrolysis of waste printed circuit boards: Comparative study of kinetics, products, and reaction mechanism. *J. Hazard. Mater.* **2022**, *431*, 128612. [[CrossRef](#)] [[PubMed](#)]
25. Cao, R.; Zhou, R.; Liu, Y.; Ma, D.; Wang, J.; Guan, Y.; Yao, Q.; Sun, M. Research on the pyrolysis characteristics and mechanisms of waste printed circuit boards at fast and slow heating rates. *Waste Manag.* **2022**, *149*, 134–145. [[CrossRef](#)] [[PubMed](#)]
26. Qin, L.; Han, J.; Zhao, B.; Wang, Y.; Chen, W.; Xing, F. Thermal degradation of medical plastic waste by in-situ FTIR, TG-MS and TG-GC/MS coupled analyses. *J. Anal. Appl. Pyrol.* **2018**, *136*, 132–145. [[CrossRef](#)]
27. Li, C.; Liu, C.; Xia, H.; Zhang, L.; Liu, D.; Shu, B. Catalytic pyrolysis of waste printed circuit boards to organic bromine: Reaction mechanism and comprehensive recovery. *Environ. Sci. Pollut. R.* **2023**, *30*, 108288–108300. [[CrossRef](#)]
28. Han, L.; Wang, Q.H.; Ma, Q.A.; Yu, C.J.; Luo, Z.Y.; Cen, K.F. Influence of CaO additives on wheat-straw pyrolysis as determined by TG-FTIR analysis. *J. Anal. Appl. Pyrol.* **2010**, *88*, 199–206. [[CrossRef](#)]
29. Hammoud, H.; Schmitt, M.; Bihel, F.; Antheaume, C.; Bourguignon, J.J. Direct Guanidinylation of Aryl and Heteroaryl Halides via Copper-Catalyzed Cross-Coupling Reaction. *J. Org. Chem.* **2012**, *77*, 417–423. [[CrossRef](#)]
30. Pan, Y.; Xu, L.; Huang, L.; He, W.; Li, H.; Wang, S.; Long, Z.; Sun, Z. Identification of Active Sites in Pt-Co Bimetallic Catalysts for CO Oxidation. *ACS Appl. Energy Mater.* **2021**, *4*, 11151–11161. [[CrossRef](#)]
31. Kim, T.; Kim, J.; Song, H.; Kim, D.; Jeong, B.; Lee, J.; Shin, J.; Ryoo, R.; Park, J. Catalytic Synergy on PtNi Bimetal Catalysts Driven by Interfacial Intermediate Structures. *ACS Catal.* **2020**, *10*, 10459–10467. [[CrossRef](#)]
32. Wu, C.; Liu, C.; Su, D.; Xin, H.; Fang, H.; Eren, B.; Zhang, S.; Murray, C.; Salmeron, M. Bimetallic synergy in cobalt–palladium nanocatalysts for CO oxidation. *Nat. Catal.* **2019**, *2*, 78–85. [[CrossRef](#)]
33. Altarawneh, M.; Ahmed, O.H.; Jiang, Z.T.; Dlugogorski, B.Z. Thermal Recycling of Brominated Flame Retardants with Fe<sub>2</sub>O<sub>3</sub>. *J. Phys. Chem. A* **2016**, *120*, 6039–6047. [[CrossRef](#)] [[PubMed](#)]
34. Ahmed, O.H.; Altarawneh, M.; Al-Harashsheh, M.; Jiang, Z.T.; Dlugogorski, B.Z. Recycling of zincite (ZnO) via uptake of hydrogen halides. *Phys. Chem. Chem. Phys. PCCP* **2018**, *20*, 1221–1230. [[CrossRef](#)] [[PubMed](#)]
35. Tang, H.; Su, Y.; Zhang, B.; Lee, A.; Isaacs, M.; Wilson, K.; Li, L.; Ren, Y.; Huang, J.; Haruta, M.; et al. Classical strong metal–support interactions between gold nanoparticles and titanium dioxide. *Sci. Adv.* **2017**, *3*, e1700231. [[CrossRef](#)]
36. Kim, D.; Park, D.; Song, H.; Jeong, B.; Lee, J.; Jung, Y.; Park, J. Metal Encapsulation-Driven Strong Metal–Support Interaction on Pt/Co<sub>3</sub>O<sub>4</sub> during CO Oxidation. *ACS Catal.* **2023**, *13*, 5326–5335. [[CrossRef](#)]

**Disclaimer/Publisher’s Note:** The statements, opinions and data contained in all publications are solely those of the individual author(s) and contributor(s) and not of MDPI and/or the editor(s). MDPI and/or the editor(s) disclaim responsibility for any injury to people or property resulting from any ideas, methods, instructions or products referred to in the content.